CHAPTER 7

MESOPOROUS OF BIOACTIVE GLASS AND GLASS-CERAMICS: INFLUENCE OF THE LOCAL STRUCTURE ON THE BEHAVIOR OF IN VITRO BIOACTIVITY

7.1 INTRODUCTION

The discovery of bioactive glass and glass-ceramics by Hench nearly three decades ago has been subject of intensive research for the materials science community, since then these classes of material promote the bone tissue regeneration, and accelerating the various healing processes. The glass developed by Hench was based on quaternary silicate system also known as 45S5® bioglass includes alkali and alkaline-earth oxide, which is considered to be the one of the best bioactive glass due their enhanced angiogenious and up-regulation of specific genes that controls the osteoblast cell cycle. The bioactive characteristics stemming from the formation of a biomimicing calcium-deficient hydroxycarbonate apatite (HCA) layer at the surface of implanted biomaterial in the presence of physiological fluid [1,2]. The HCA layer has an identical chemical composition as the inorganic constituents of bones and dentin. The usefulness of a bioactive glass strongly depends on the rate at which HCA forms on its surface; if the rate of HCA formation is slow then the material is said to be bioinert. More commonly, the development of HCA layer is assessed by in vitro test using a simulated body fluid (SBF), it initially forms an amorphous calcium phosphate phase followed by crystallization. Thus, the formation of amorphous HCA layer and subsequent mineralization is highly dependent on the numerous factors such as chemical composition, textural properties and ion dissolution kinetics.

Bioactive glasses and glass-ceramics (GC) have been the subject of intensive research in biomedical applications since their discovery 40 years ago. Most widely applied bioactive glasses and glass-ceramics consist of silicate network incorporating sodium, calcium, phosphorus in different relative proportions in the SiO_2-Na_2O-CaO-P_2O_5 systems [3]. After development of bioglass 45S5® by Hench in 1971[4], various research groups have started developing new materials with better mechanical strength, to

be used in load-bearing positions. In this context, the GC such as Ceravital®, Cerabone®, Ilmaplant®-L1 and Bioverit® are some of the glass ceramics developed in the recent decades [5-7]. These bioactive GC have good mechanical properties but relatively low bioactivity indexes. With the development of sol-gel technique [8] and hierarchal mesoporous structure [9], the focus has been shifted to development of porous bioactive glasses and glass-ceramics due to their excellent properties. Recently, Chen et al successfully synthesized porous, mechanically competent, bioactive and biodegradable glass-ceramic with composition close to 45S5 [10].

The discovery of M41S materials synthesized with surfactant template method by the research group of Mobil Oil Corporation in 1991,[11] the mesoporous silica has received much attention due to its excellent properties in numerous applications[12,13]. More commonly, the silica-based mesoporous materials (SMM) are characterized as having high surface area, pore volume and pore size, with narrow pore size distribution, and high surface silanol density which confer the necessary requisites to behave as bioactive materials. Furthermore, in vitro assays were performed on SBA-15, MCM-48 and MCM-41 and observed that high surface area and high silanol density are not enough to promote bioactive behavior [14]. As a result various strategies were employed [15,16] to accelerate the bioactive response of SMM. In practice, significant advancement has been achieved in this field when the sol-gel syntheses of SiO_2-CaO-P_2O_5 glasses were prepared with outstanding textural properties along with an ordered pore arrangement[17]. By retaining such mesostructured glasses show the exceptional growth for monoclinic-like HCA in SBF with shorter period of time. However, there are several issues of these mesostructured glasses debated, such as correlation between the textural property and apatite formation, as well as the mechanistic details of surface reactions involved. Apart from highly ordered mesoporous structures, less ordered wormhole-like mesoporous materials has also been recently developed [18], which shows nearly similar properties of ordered mesoporous material. The channel branching within the network structures in these less ordered materials also show better performance in certain circumstances[19].

In order to understand the various aspect of HCA layer formation different experimental techniques such as X-ray diffraction (XRD), Fourier transform infrared (FTIR) and nuclear magnetic resonance (NMR) spectroscopy, and different microscopic techniques has been explored[20-25]. These experimental techniques tend to be very useful in investigating the surface reactions at each stage of reactions involved in HM, starting from leaching of ions to HCA formation. More recently, Aina et al very well investigated the modifications of the surface composition upon reaction as well as the deposition of Ca-P layer and the consequent crystallization to HCA at the MBG surfaces [26]. Additionally, the combined NMR and HRTEM investigations has been carried out to probe the mechanism of apatite mineralization and reveals that the surface reactions observed in MBG's are contrasted with HM. Since, the HM of apatite formation is more applicable for traditional melt-derived bioactive glass (MDBG) owing to the local atomic structure, and poor textural nature [27].

Based on the obtained experimental results different conclusions has been made to correlate the local structure and formation of the HCA layer. However, many details of the bioactive glasses, such as inter correlation between the chemical composition and HCA layer formation and surface reactions involved in it are debated. Furthermore, more importantly the exact conversion between amorphous calcium phosphate and the ultimate crystalline HCA product poorly understood. In this context, computer simulation techniques has been exploited, which predicts the bioactive behavior of bioglasses and local atomic structure [28]. In particular, the work done by Tilocca and his co-workers by molecular dynamics simulation study offers fundamental understanding of structure of complex nature of 45S5 glass and few other glass compositions [29].

In this work, we report for the first time the synthesis of mesoporous sodium oxide containing bioactive glass and glass ceramic in SiO_2-Na_2O-CaO-P_2O_5 quaternary system by sol-gel method followed by EISA process. As prepared glasses possess high surface area, pore volume and narrow pore size distribution, which exhibits excellent in-vitro bioactive behavior revealed by BET surface area analyzer. In particular, we discuss the variation in structural, textural and morphological properties with the addition of calcium oxide content. However, with an increase of

calcium oxide content above 30 mol%, we get a glass-ceramic which consists of three phases i.e. apatite, wollastonite and residual glassy phase. An obtained glass and glass-ceramic samples are characterized by various experimental techniques to obtain local atomic structure. Moreover, we also discuss the influence of chemical composition, local atomic structure as well as dependence of textural properties on bioactive behavior of the mesoporous glasses and glass-ceramics.

7.2 EXPERIMENTAL SECTION

7.2.1 Materials and Method

Mesoporous bioactive silicate glasses (MBGs) of quaternary system with different chemical compositions as listed in Table 7.1 were prepared by means of acid assisted sol-gel route followed by EISA process. The following chemicals were used as precursors for synthesis of MBGs: Tetraethyl orthosilicate (TEOS) (Aldrich 99%), sodium acetate (NaAc) (Sigma Aldrich 99%), calcium acetate (CaAc), Triethylphosphate(TEP), Ethanol (AR, china),Acetic Acid, non-ionic amphiphilic triblock copolymer (P123) that has following sequence: $EO_{20}PO_{70}EO_{20}$, where EO is poly (ethylene oxide) and PO is poly(propylene oxide) (Aldrich) (M_w=5800), and Deionised water (DI). Briefly, the molar ratios of TEOS, TEP, NaAc and CaAc were designed according to molar ratio of SiO_2, Na_2O, CaO, P_2O_5 content. In order to achieve clear sol P123, TEOS,TEP, NaAc, CaAc and acetic acid were dissolved in ethanol after one hour interval and stirred at room temperature for 24 hrs and the corresponding molar ratio of TEOS/TEP: ethanol=1:4, TEOS/TEP: water=1:4 and weight ratio of water: acid=1:6. The resulting sol was then introduced into the petridish to undergo EISA process. Following this, as evaporated gel was aged for 3 days and then dried at 100 ^oC for 48 hrs. Additionally, we have adopted the acid treatment for template removal and calcinations at 400^oC for 4 hrs.

7.2.2 Characterization

The as prepared samples were characterized by WAXRD, SAXS, FTIR, and N_2-sorption techniques. The *in vitro* bioactivity of as prepared samples was carried out immersing them in SBF with ionic concentration nearly equal to the human blood

plasma at different intervals. An evolution of the SBF concentrations was monitored by means of pH value caused by the ion exchange processes between bioactive glass and the surrounding medium. Additionally, the ion concentration of the SBF solution after the removal of SBF soaked glass and glass-ceramic sample was analyzed by inductive coupled plasma (ICP) atomic emission spectroscopy. The surface morphology of soaked samples were characterized by XRD, FTIR, SEM, and N_2-SORPTION techniques to study the evolution of apatite layer.

High resolution MAS-NMR spectra glass and glass-ceramics were acquired at room temperature using Bruker DSX-300 spectrometer operating at 121.49 (^{31}P signal) and 59.62 MHz (^{29}Si signal) with field strength of 7.04 T. The ^{29}Si MAS-NMR spectra were made of 2048 free induction decays (FID) with a 30^o pulse of 2.5 μs and a relaxation decay of 5 s. The ^{31}P MAS-NMR spectra were recorded at 512 scans with a 45^o pulse of 3.5 μs and a relaxation decay of 5 s. The chemical environment of two different nuclei: silicon ^{29}Si and phosphorous ^{31}P were recorded with respect to tetramethylsilane (TMS) as reference for ^{29}Si spectra and H_3PO_4 (85%) solution as reference for ^{31}P spectra. All the samples were spun at the magic angle of 54.7^o and at the spinning rate of 5-8 kHz on finely ground powders filled in 5 mm zirconia rotors. The experimental errors in the chemical shifts were ±0.1 ppm for ^{29}Si and ±0.5 ppm for ^{31}P signals. A deconvolution procedure was performed to obtain quantitative estimation of Q^n species on the base-line corrected spectrum.

7.3 RESULTS AND DISCUSSION

7.3.1 Structure, Morphological and Textural Characterization

As prepared glass and glass-ceramic samples are characterized by XRD, FTIR, NMR, TEM, Nitrogen sorption technique to get detailed insights on their structural, morphological, and textural properties which aids to understand their role in bearing on the bioactivity. WAXRD patterns of 73S10C, 63S20C and 53S30C samples are shown in Figure 7.1. More commonly, the broad hump is associated with the characteristic amorphous nature in the case of 73S10C and 63S20C samples. Whereas, in 53S30C sample amorphous feature partially disappeared and Bragg reflections corresponding to calcium phosphate hydroxide-type phase [$Ca_5(PO_4)_3(OH)$] (JCPDS 03-0348) and

wollastonite [$CaSiO_3$] (JCPDS-84-0655) has been indentified (Figure 1). Based on the XRD results, we confirm that 50S30C composition is found to be glass-ceramic with two different crystalline phases: hydroxyapatite and wollastonite and a residual glassy phase as observed in Cerabone® A/W. It is worthwhile to mention that the bioactivity index of Cerabone® A/W roughly one-fourth of bioglass 45S5® [30].Furthermore, the broadening of XRD pattern indicates that in 53S30C glass-ceramic the crystallites are nanocrystalline in nature.

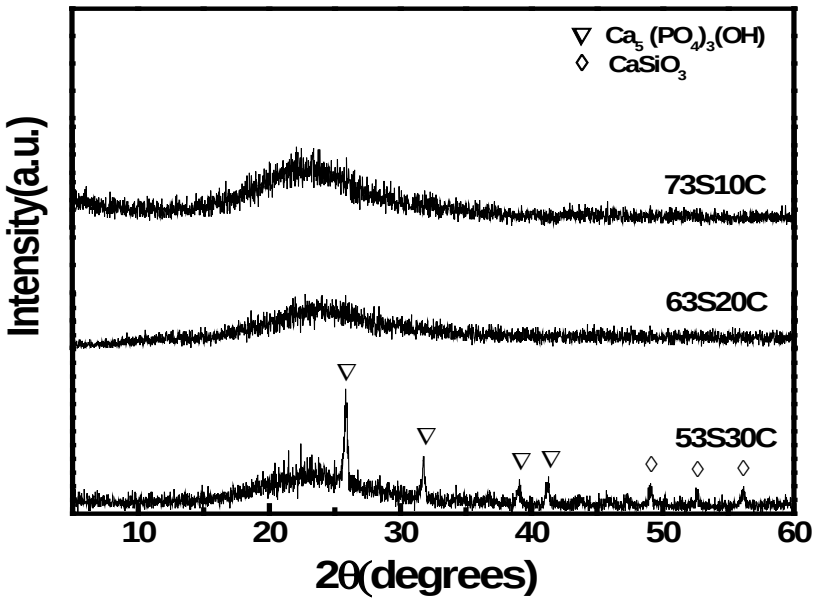

Figure 7.1: *WAXRD patterns of 73S10C, 63S20C and 53S30C before soaking in SBF.*

In Figure 7.2, we present the FTIR spectra of 73S10C, 63S20C glass and 53S30C glass-ceramics. The FTIR spectra of both the glass samples show a broad absorption band at 1630 cm^{-1} attributed to the adsorption of water in the form of hydroxyl groups [31]. Additionally, the existence of hydroxyl groups resulting from the hydration of sol-gel glasses is indicated by vibration of band at 970 cm^{-1}, assigned to non-bridging oxygen (NBO's) together with the surface silanols (Si-OH) groups which enhances the rate of apatite formation. The surface silanol groups are further confirmed by presence of a broad band in the region 3000-3770 cm^{-1}, which represents the vibration of different hydroxyl groups. In all the samples, the vibrational spectra shows the characteristic absorption bands of Si-O-Si asymmetric stretching vibration (1300-900 cm^{-1}), Si-O bending vibration around 800 cm^{-1}, and Si-

O-Si symmetric stretching vibration around 470 cm^{-1}. The weak intensity peak around 560 cm^{-1} show the presence of amorphous calcium phosphate (Ca-P) clusters on the silica walls [32]. This signifies that presence of the Ca-P moieties in the virgin samples would accelerate the bioactive behavior of these materials [33].

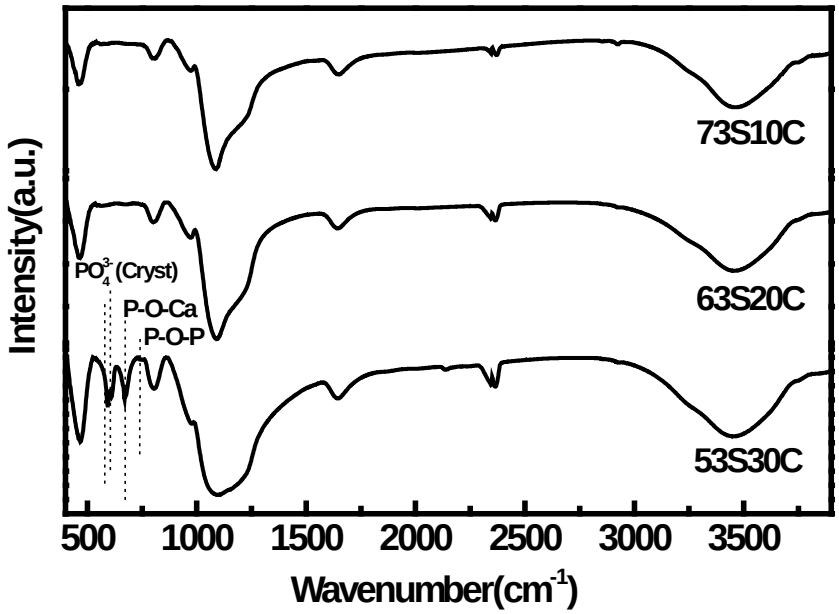

Figure7.2: *FTIR Spectra of 73S10C, 63S20C and 53S30C before soaking in SBF.*

The mesoporous 73S10C, 63S20C glass and glass ceramics 53S30C showed the Si-O-Si asymmetric stretching vibration centered at 1088, 1090 and 1098 cm^{-1} respectively which is lower than that of pure silica located at 1123 cm^{-1} and a shoulder around 1220 cm^{-1}. The shift in the band position can be attributed to changes in the Si-O-Si bond angle, which depends on the effect of metal cation in the silicate glass structure[34,35] and can also be attributed to presence of orthophosphate units associated with Ca^{2+} [36]. Apart from the Si-O-Si characteristic bands, 53S30C mesoporous glass-ceramic sample show the absorption band doublet at 592 cm^{-1} and 610 cm^{-1} characteristic of $(PO_4)^{3-}$ units and a strong absorption band at 670 cm^{-1} and a weak band at 748 cm^{-1} corresponding to vibrations of P-O-Ca and P-O-P bonds respectively [37]. Based on these vibrational bands, we ascertain the existence of hydroxyapatite type phase in the obtained glass-ceramic composition. The observed vibrational bands between 580-620 cm^{-1} co-inside with the occurrence of $CaSiO_3$ wollastonite phase as well. Therefore, broadening of the band centered at around 1090

cm^{-1} increase with CaO content, which signifies the presence of phosphate vibrational modes overshadowed by silicate bands [38].

The nitrogen adsorption/desorption isotherms and pore size distribution curves are shown in Figure 7.3 and the estimated textural parameter values are listed in Table 7.1. As prepared glass samples exhibit a type IV isotherm, typical for mesoporous materials with H1 type hysteresis loop characteristic of cylindrical pore channels with the narrow pore size distribution [39].

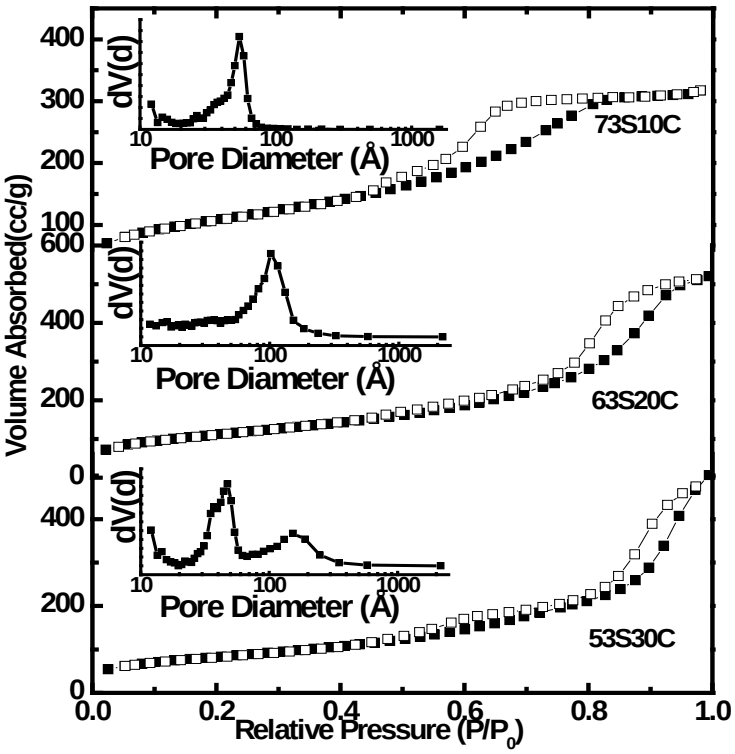

Figure 7.3: *Nitrogen sorption isotherms and pore size distribution (inset) of 73S10C, 63S20C and 53S30C before soaking in SBF.*

Table 7.1: *Chemical composition and textural parameters*

Sample	Composition (mol %)				Surface area ($m^2.g^{-1}$)	Pore size (nm)	Pore volume ($cc.g^{-1}$)
	SiO_2	Na_2O	CaO	P_2O_5			
73S10C	73.4	14	10	2.6	398	5.4	0.522
63S20C	63.4	14	20	2.6	371	10.3	0.762
53S30C	53.4	14	30	2.6	294	4.9,15.6	0.806

The BET surface area of the sample changes with the calcium content and reaches around 398 m^2/g for glass with 10 mol % of CaO and around 294 m^2/g for the glass ceramic composition, which is relatively larger than the reported values of the quaternary glass and glass-ceramic systems in the literature [40,41]. The pore size distribution curves are derived from the adsorption branch of the isotherm using BJH model, which represents relatively narrow range and monomodal type distributions. The increase in the pore size with calcium content is due to the depolymerization of the silicate network structure. Thus, the enhanced textural properties can accelerate in vitro bioactivities of these glasses [42].Whereas, in 53S30C the isotherm has a pronounced double hysteresis loop, as seen in Figure 7.3 and the pore size distribution shows clearly the bimodal distribution due to the presence of two types of phases: the crystalline phase consists of apatite and wollastonite and residual glassy phase as observed in XRD pattern.

In order to determine the local environments of the network forming species on these samples at the atomic level, a study by NMR has been undertaken. In Figure 7.4, illustrates the ^{29}Si MAS-NMR spectra of all three samples, to obtain local structural speciation of various Q^n species in glass and glass-ceramic. Here, we adopt Q^n notation to denote silicon and phosphorus atom bonded to n bridging oxygen (BO's) and (4-n) non-bridging oxygen (NBO's) atoms.

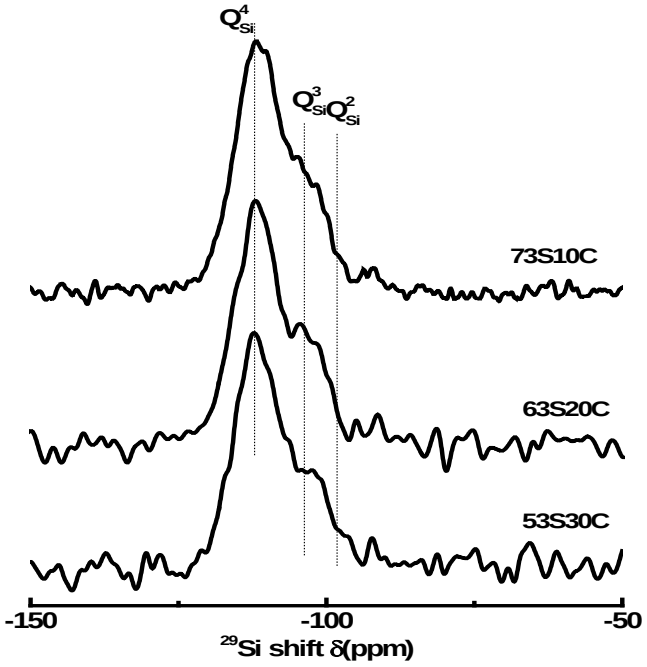

Figure 7.4: *^{29}Si MAS-NMR spectra of representative pristine sol-gel glasses and glass-ceramic.*

All the pristine samples are dominated by a broad band centered at -112 ppm assigned to Q^4_{Si} species, which form the three dimensional network structures. The spectral assignments are less obvious because of competing roles of network modifier and H^+ for charge compensating the NBOs present. In bulk alkali and alkaline-earth modified silicate glasses the chemical shift values for Q^2_{Si}(Na) is assigned at -76 ppm and Q^2_{Si}(Ca) at -83 ppm [43]. However, we don't observe any spectral features at these chemical shift values in the obtained raw spectra of present glass compositions. In order to evaluate more qualitatively the variation of individual Q^n species with CaO content, we have followed the deconvolution procedure and identified the species associated within the glass and glass-ceramics. On the deconvoluted spectra's, we find that there are two major components correspondingly the Q^4_{Si} and Q^3_{Si} species and a minor amount of Q^2_{Si} species due to the depolymerization of silica network (Figure 7.5). The MBGs which involves Q^3_{Si} and Q^2_{Si} structural units are more commonly associated with $Si(OSi)_3OH$ and $Si(SiO)_2(OH)_2$ groups due to the presence of silanols (-OH) groups [44,45]. It has been observed more qualitatively that the relative proportion of Q^3_{Si} band decreases in relation to reduction in the modifier concentration.

Table 7.2: *Relative populations (expressed as percentages) of Q^n_{Si} species obtained after deconvolution of the obtained spectra.*

Sample	Q^4_{Si}(A)		Q^3_{Si}(B)		Q^2_{Si}(C)	
	δ(ppm)	Area(%)	δ(ppm)	Area(%)	δ(ppm)	Area(%)
73S10C	-111.58	78	-102.3	20	-92.6	2
63S20C	-111.60	73	-102.2	23	-92.3	4
53S30C	-111.8	68	-101.9	25	-92.4	7

In Table 7.2, we list the relative populations (expressed as percentages) of Q^n_{Si} species obtained from deconvolution of all the spectra's. The variation of silica Q^n-species in these glasses and glass ceramic evidences the effect of network modifiers on the silicate network.

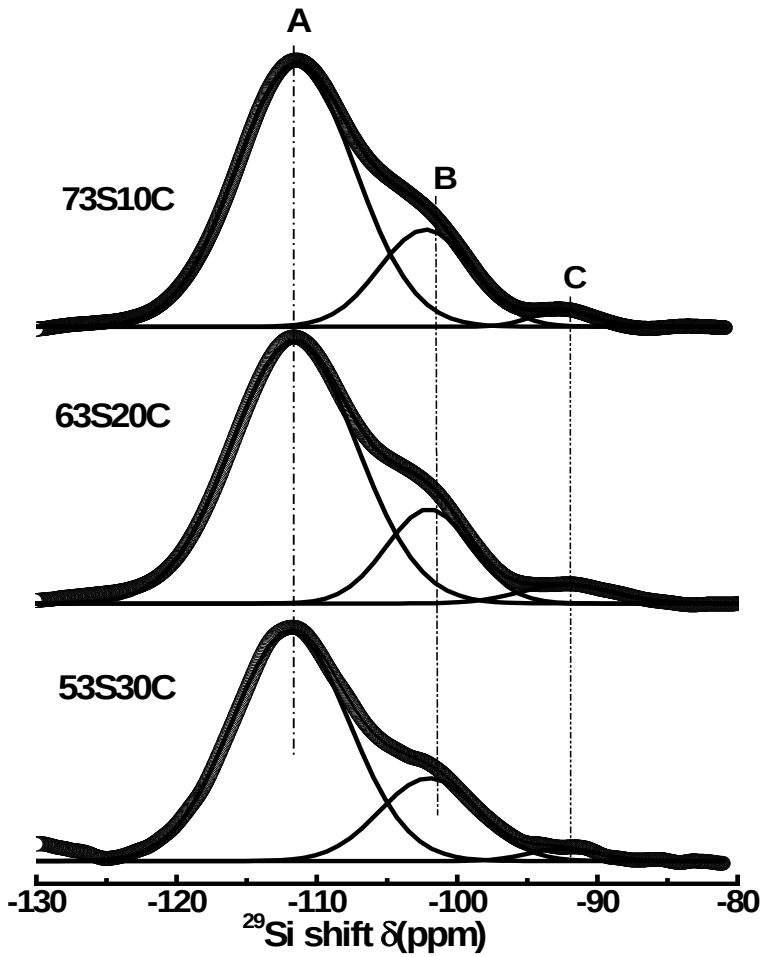

Figure 7.5: *^{29}Si Spectra for pristine glasses and glass ceramic after deconvolution into various Q-species for silica. (Open circle represents the obtained spectra and solid line represents deconvoluted spectra).*

Figure 7.6 shows the ^{31}P MAS-NMR spectra of pristine 73S10C, 63S20C and 53S30C samples with distinguishable features. In order to get the detailed insights on the type of Q_p^n species present in the glass and glass-ceramic samples, the ^{31}P NMR spectra are deconvoluted and fitted to Guassian lines as shown in Figure 7.7. The chemical shift values and the percentage of population (peak area) of individual species after deconvolution of the ^{31}P spectra are summarized in Table 7.3. Clearly, 73S10C glass sample ^{31}P NMR spectra exhibits four resonance peaks at -3.1, -1.4, 0 and 1.2 ppm as shown in Figure 7.6. The observed resonance peak around -3.1 ppm lie between the ^{31}P chemical shift of $Ca_2P_2O_7$ (-7 ppm) and $Na_4P_2O_7$ (2.9 ppm) suggesting that phosphorous exists as pyrophosphate Q_p^1 complex with mixed sodium and calcium environment [46,47]. The chemical shift at -1.4 ppm and 1.2 ppm could be assigned to dicalcium

phosphate dehydrate (Monetite, $CaHPO_4$) and dicalcium phosphate dihydrate (Brushite, $CaHPO_4.2H_2O$) due to the presence of large amount silanol and molecular water content [48,49], whereas the resonance peak around 0 ppm could be attributed to pure calcium orthophosphate phase [50]. The presence of Q_p^1 species is the most apparent from the 70S10C spectra which confirms the possible P-O-Si bonding existence in this glass composition. Recently, Leonova et al [51] suggested that this signal is derived from P-O-Si moieties stemming from P clusters at spots of silica-based pore-wall surface.

In 63S20C glass sample, the deconvoluted ^{31}P spectra reveals that the major resonance band occurs at 0 ppm and it is attributed to calcium orthophosphate (Q_p^0) species. The two weak bands corresponding to chemical shifts -1.7 ppm and 1.6 ppm again signify the presence of both Monetite and Brushite phases, respectively. This may be rationalized by suggesting that introduction of Ca is associated with a concurrently enhanced water adsorption and hence form hydrated calcium phosphate structure.

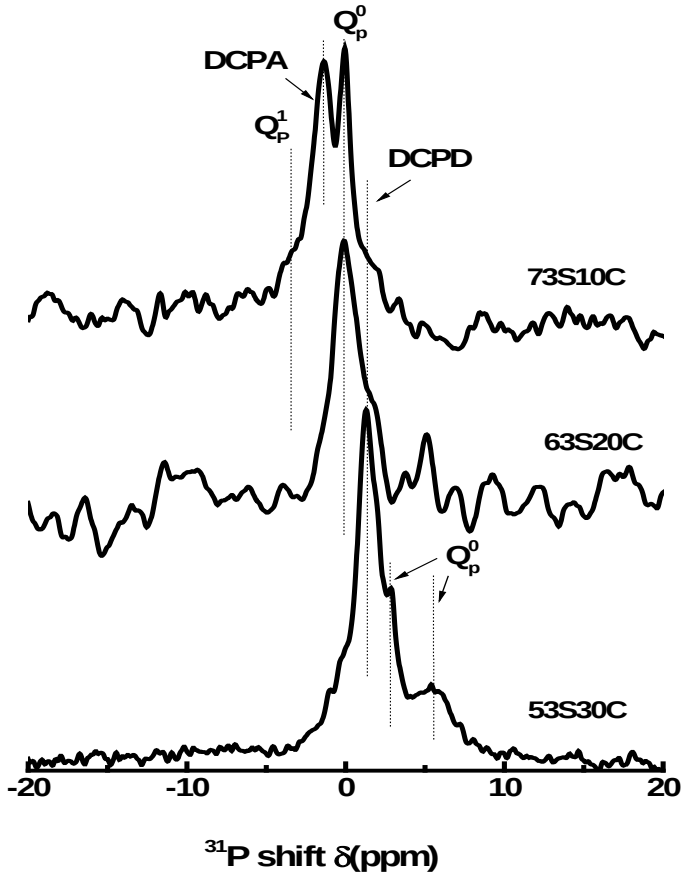

Figure 7.6: *^{31}P MAS-NMR spectra of representative pristine sol-gel glasses and glass-ceramic. (DCPA: Dicalcium phosphate anhydrous or dehydrate and DCPD: Dicalcium phosphate Dihydrate).*

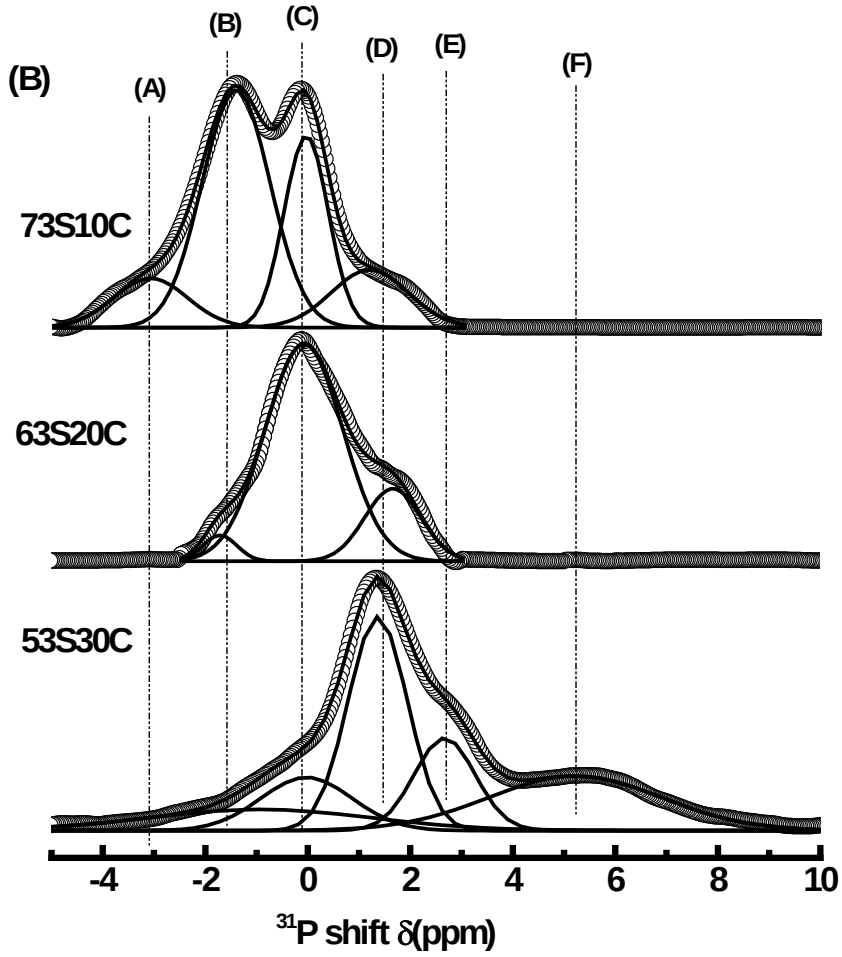

Figure 7.7: *^{31}P Spectra for pristine glasses and glass ceramic after deconvolution into various Q-species for phosphate.(Open circle represents the obtained spectra and solid line represents deconvoluted spectra).*

Table 7.3: *Relative populations (expressed as percentages) of Q_P^n species obtained after deconvolution of the obtained spectra.*

Sample	Q_p^1(A)		Monetite (B)		Q_p^0(C)		Brushite (D)	
	δ (ppm)	Area (%)	δ (ppm)	Area (%)	δ (ppm)	Area (%)	δ (ppm)	Area (%)
73S10C	-3.1	11	-1.4	50	0	25	1.2	14
63S20C			-1.6	19	0	71	1.6	10
53S30C			-0.9	13	0	38	1.4	9

Sample	Q_p^0(HAp) (E)		Q_p^0(Na,Ca) (F)	
	δ (ppm)	**Area (%)**	**δ (ppm)**	**Area (%)**
73S10C				
63S20C				
53S30C	2.7	15	5.2	25

It is interesting to note from the ^{31}P spectra of 53S30C glass-ceramic sample, we observe the five distinct chemical shift values between -1 and 5.5 ppm. The obtained chemical shift values for individual band positions and the percentage of areas under the peak are listed in Table 7.3. The chemical shifts around -0.9 ppm and 1.3 ppm corresponding to Monetite and Brushite phases i.e. the dehydrated or anhydrous dicalcium hydrogen phosphate amount is more in comparison to brushite phase owing to scarce amount of molecular water and silanol groups in the glass-ceramic sample. The chemical shift values around 0 ppm, 3 ppm and 5.5 ppm are assigned to Q_p^0 species corresponding to orthophosphate but with different neighbors. More commonly, the chemical shift at 0 ppm is associated to calcium orthophosphate [47], whereas the chemical shift at 3ppm is again same as that of crystalline calcium hydroxyapatite [51, 40] and in the present case, it is due to the presence of Ca-P clusters or hydroxyapatite environment [52,53]. It is worth to mention that this chemical shift value in similar to that reported in Ca-rich bioactive glasses, where the ^{31}P signal appears around 2.5-3.0 ppm is attributed to orthophosphate environment [43]. The observed chemical shift around 5.5 ppm which lie between sodium orthophosphate (16 ppm) and calcium orthophosphate (0-3ppm) suggests that the phosphate exists as mixed sodium-calcium orthophosphate environment [51], i.e. both types of modifier ion are associated with the orthophosphate units. Thus, the ^{31}P MAS-NMR spectra analysis underline the fact that phosphorus is conventionally thought to enter as network former however, here we find that it exists as isolated orthophosphate structural units.

7.3.2 In Vitro Bioactivity Test

The bioactivity of glass and glass ceramics has been carried out by analyzing both the as prepared glass powder and the supernatant SBF solution. The in vitro apatite formation and changes in the chemical composition i.e. the ion concentration of the SBF solution after soaking the samples for different durations were systematically monitored. The chemical composition of the SBF solution after soaking was monitored by ICP-AES analysis as a function of soaking time. The chemical concentrations of individual ionic species released in SBF solution for 73S10C and 53S30C samples after soaking in SBF for 12 hr, 1day and 3 days at the ppm level are calculated and reported in Figure 7.8. It is evident that the Ca species initially (12 h) show rapid release followed by decrease in concentration with time and this behavior become more prominent in 73S10C glass than 50S30C glass-ceramic sample. Thus, the initial increase in Ca^{2+} concentration could be due to Ca^{2+} release from the soaked sample. The subsequent decrease in the Ca^{2+} concentration with the immersion time is attributed to the formation of the amorphous calcium phosphate layer over hydrated silica-rich layer forming negative potential at the glass surface, necessary to incorporate Ca^{2+} ions from the SBF solution to the surface and forming crystalline Ca-P [54]. The change in P concentration follows the similar trend in both samples but 53S30C sample release less phosphorus in comparison with other two glass samples, which show that apatite formation ability become difficult in this composition. The reason for the slow ion dissolution of Ca and P in 53S30C sample is the presence of different phases and phase boundaries. Therefore, the dissolution of ionic species depends solely upon the type of phase in which ions are trapped as well as their textural nature [55]. All the composition shows an increase in Si concentration during the soaking period, which indicates that Si continuously leached from the MBG's through the breakdown of the mesoporous structure and further leads to the degradation of bioactive glass [56].

The immersion of samples in SBF solution also results in an appreciable increase in Na^+ concentration which indicates that there is an exchange of Na^+ ions with the H_3O^+ present in the fluid. Therefore, the mesoporous glass samples accelerate the formation of Si-OH groups on its surface within 12 h of the dissolution

than the glass-ceramic sample, where the Na^+ ion dissolution rate is significantly slow, which again indicates the rate of reaction kinetics of apatite formation. The amount of consumption of calcium and phosphate in the solution was calculated by subtracting the value after three days of dissolution from the 12 h dissolution and compared in Figure 7.9. This consumption data indicates that amount of CaP deposited on 73S10C glass surface after three days, i.e. the Ca/P ratio of around 1.65 very close to stoichiometric Ca/P ratio of hydroxyapatite (1.67) [57,58]. On the other hand, 53S30C glass-ceramics sample show the strong deviation (the estimated Ca/P ratio of 1.45) from the stoichiometric Ca/P ratio which suggests the formation of the more meta-stable CaP phase other than HAp compared to 73S10C glass sample [42].

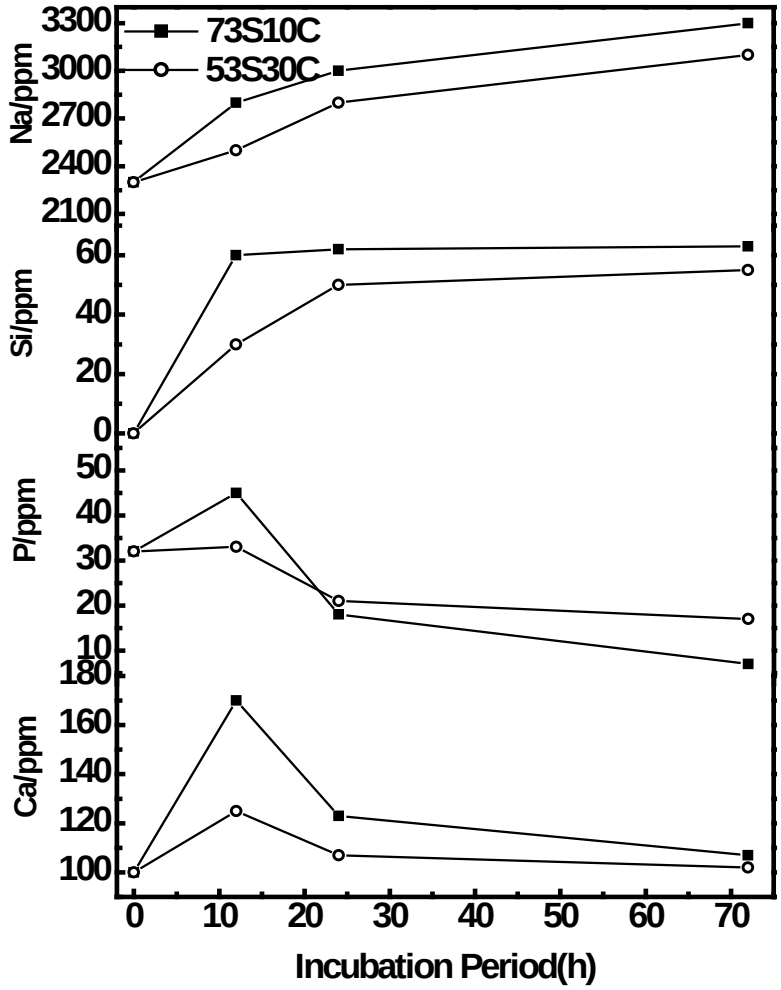

Figure 7.8: *Ca, P, Si and Na concentrations in SBF as a function of soaking time for 73S10C and 53S30C.*

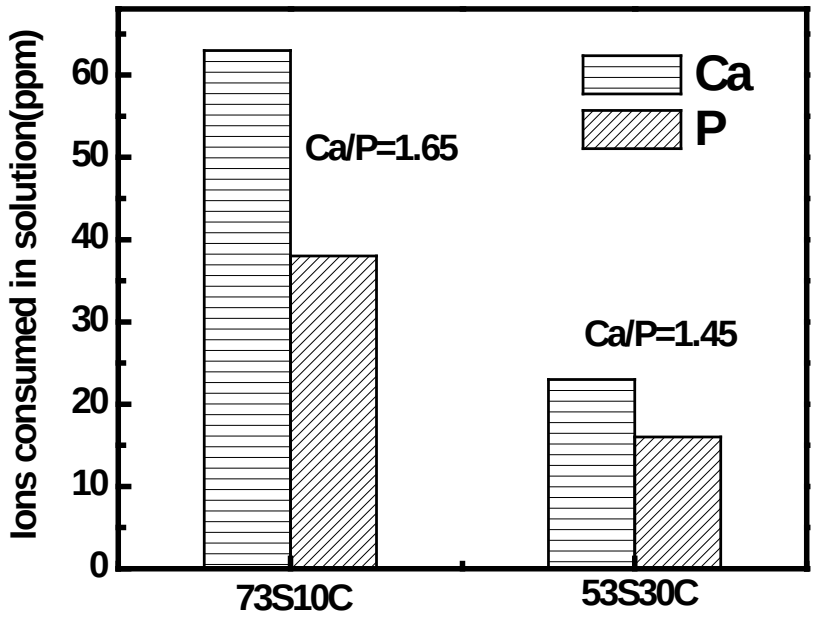

Figure 7.9: *Total consumption of Ca and P for 73S10C and 53S30C.*

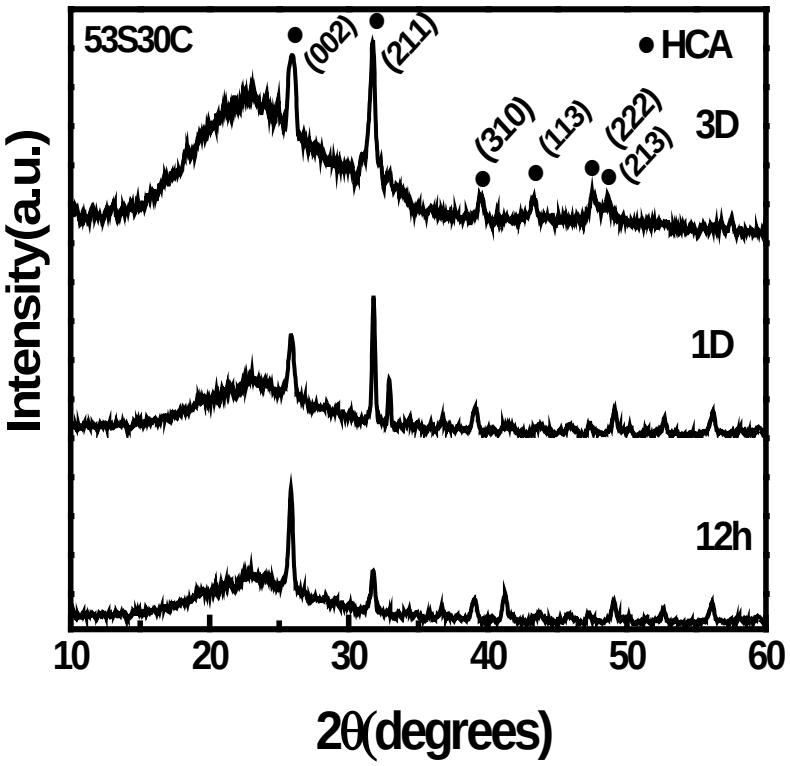

Figure 7.10: *WAXRD pattern of 53S30C after soaking in SBF for 12h, 1D and 3D.*

Furthermore, the SBF soaked samples has been characterized by the XRD analysis with different durations such as 12h, 1day and 3 days are shown in Figure 7.10 and 7.11. The initial period of soaking (12 h) leads to the appearance of less intense peak corresponds to the HCA phase and the diffraction peaks become more intense with an increase of soaking period. In the case of 73S10C sample, one day soaking period results the less intense apatite diffraction pattern appears and is indexed to (002), (211), and (222). The subsequent increase of time (three days) the diffraction peaks became more intense as well as additional peaks start appearing corresponds to (130), (131) and (213) (JCPDS-24-0033)[59]. In contrast, the structural changes on the glass-ceramic sample with respect to the apatite formation are less pronounced with the soaking time. On comparing XRD pattern of all the three samples soaked on three days, it is evident that the crystallanity of the apatite precipitate enhances in the sequence 73S10C > 63S20C > 53S30C.

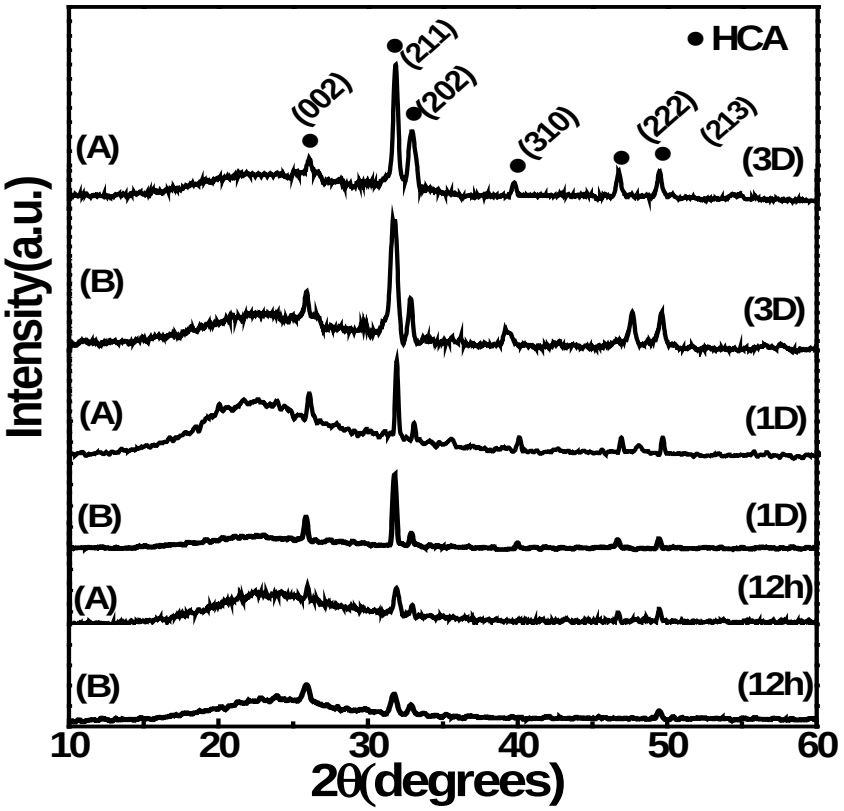

Figure 7.11: *WAXRD pattern of 73S10C(A), and 63S20C(B) mesoporous glass samples after soaking in SBF for 12h, 1D and 3D.*

Furthermore, we have confirmed the HCA formation by characterizing the SBF soaked samples using the FTIR technique and the results are shown in Figure 7.12. The in vitro bioactivity was assessed by analyzing the absorption band at 560-600 cm^{-1} with doublet in the spectra, corresponding to the formation of crystalline apatite [59]. In is interesting to note that the FTIR spectra of 73S10C sample shows the appearance of phosphate bands at 1045, 604 and 556 cm^{-1} and carbonate absorption bands at 1490, 1426 and 873 cm^{-1} after soaking in SBF for three days. Furthermore, the spectra of all the samples after soaking in SBF reveals the disappearance of 960 cm^{-1} band and a shift of 1090 cm^{-1} corresponding to Si-O-Si stretching towards lower wave number of 1045 cm^{-1}. The shift of the band at 1090 cm^{-1} to lower wavenumber corresponds to the P-O stretching mode with increasing soaking time, which again confirms the formation of apatite rich layer on the glass surface. In contrast to relatively sharp absorption bands detected in 73S10C glass sample, the FTIR spectra for 53S30C glass-ceramic shows very weak doublet peaks for the similar soaking time. Thus, the FTIR results are in corroboration with the obtained XRD results after soaking in SBF for various time durations.

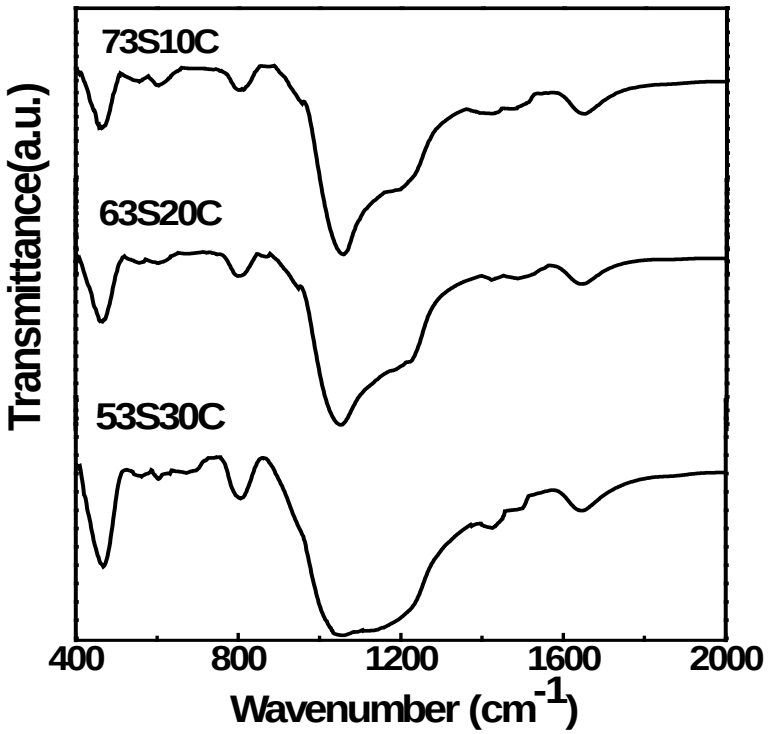

Figure 7.12: *FTIR spectra for 73S10C, 63S20C and 53S30C after soaking in SBF for 3D.*

To investigate the morphological changes on the mesoporous glass samples after SBF immersion for 12 h and three days are characterized by SEM as shown in Figure 7.13. Initially all the as-prepared samples have the smooth surface and after three days of soaking in SBF, sample surface (73S10C) becomes rough covered by a new phase composed of spherical particles (around 3μm) with small needle-like crystallites can be distinguished. In 63S20C glass sample the formed apatite phase has spherical particles with 1-2μm diameter whereas needle-like crystallites are hardly observed. Thus, these needle-like crystallites are characteristics of biomimetically grown apatite phase on the glass surface. In the case of glass-ceramic sample, the spherical particles are around 0.5-1μm in diameter and there is no evidence of needle-like structures.

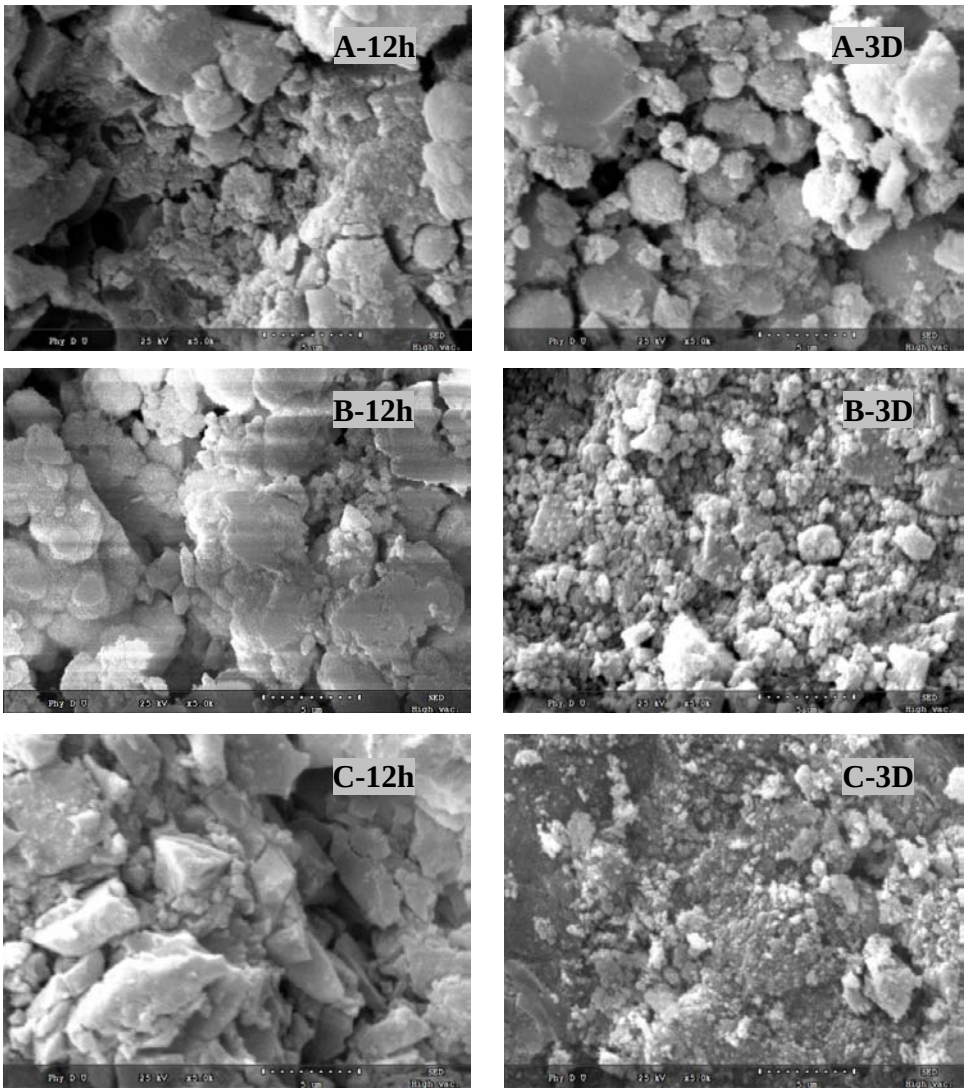

Figure 7.13: *SEM micrographs of (A) 73S10C (B) 63S20C (C) 53S30C after soaking in SBF for 12h and3D (scale-5μm).*

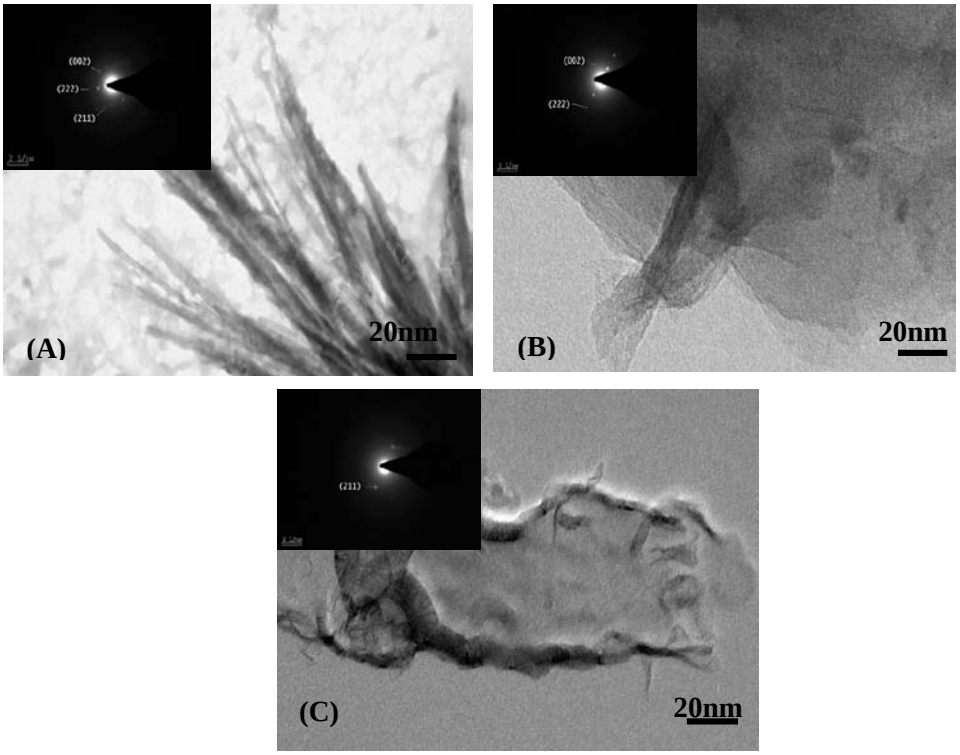

Figure 7.14: *TEM micrographs and corresponding SAED pattern of (A) 73S10C (B) 63S20C and (C) 53S30C after soaking in SBF for 3D.*

Additionally, we have carried out TEM and selected area electron diffraction (SAED) analysis of in vitro bone mineralization process on glass and glass-ceramic sample surface. Micrographs depicted in Figure 7.14 shows crystalline aggregates composed by needle-like crystals formation on the surface of glass and glass ceramic samples. The SAED pattern analysis reveals the (002), (211) and (222) reflections corresponding to apatite phase having with d-spacing of 0.34nm, 0.28nm and 0.19nm respectively [60]. The observed phases are more visible in the case of 73S10C glass than other glass and glass-ceramic samples. More specifically, the glass-ceramic sample shows the less or absence of reflections corresponding to the apatite phase. The diffuse maxima in the observed XRD pattern of glass-ceramic sample are manifested by the presence of nanocrystallites with random orientation [61].

The nitrogen sorption isotherms and the corresponding pore size distribution curves for 73S10C, 63S20C and 53S30C samples after SBF soaking for three days are illustrated in Figure 7.15. The obtained textural parameters extracted from the physiosorption data are listed in Table 7.4. By comparing the adsorption curves, it is

evident that all isotherms are identified as type IV with similar H1 Type hysteresis loop. However, the relative pressure at which the hysteresis and capillary condensation occurs is different from those of pristine samples as well as the change in the isotherm become apparent with CaO content. Additionally, it is interesting to note that the appearance of double hysteresis in 53S30C glass ceramic sample then in pure glass samples. The surface area and pore volume decreases to some extent after soaking in SBF which may be due to the formation of hydroxyapatite phase partially in the mesoporous channels. The pore size distribution curves from the adsorption branch shown in inset of Figure 7.15 reveals bimodal distribution. The absolute values of pores range from 5-7 nm for 73S10C and 4-13nm for 63S20C glass samples, which indicates that some of the pore channels are retained even after soaking [62]. In the case of glass-ceramic sample (53S30C), multimodal pore size distribution with ranging from 3 - 16nm has been observed. The large pore size distribution is due to the leaching or dissolution of ions from different phases such as apatite-like, wollastonite and residual glassy phase [63].

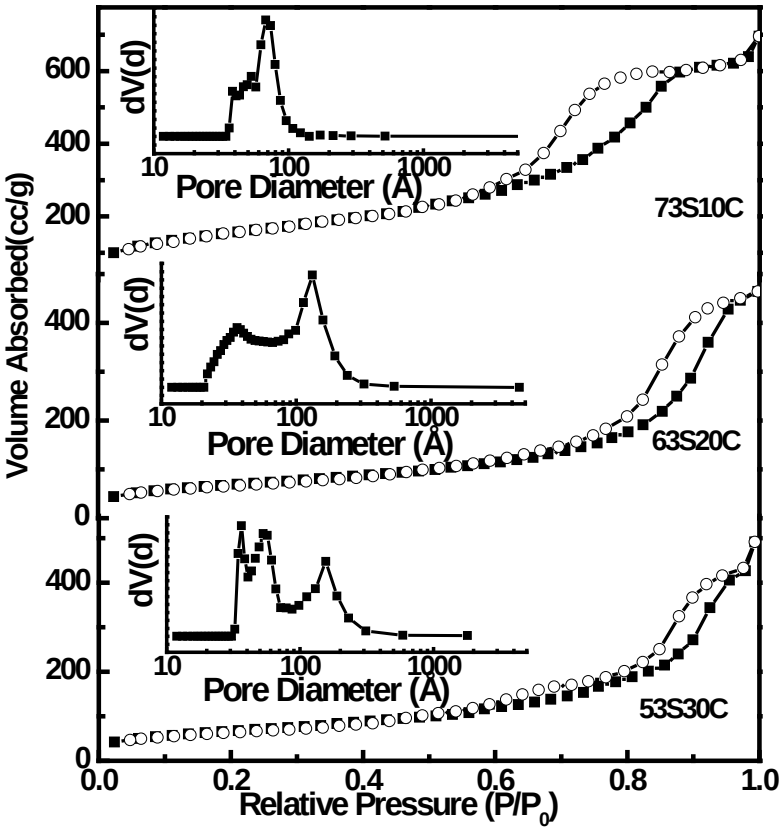

Figure 7.15: *Nitrogen sorption isotherms and Pore size distribution (inset) of 73S10C, 63S20C and 53S30C after soaking in SBF.*

Table 7.4: *Textural parameters of samples after soaking in SBF for 3days.*

Sample	Surface Area ($m^2.g^{-1}$)	Pore size (nm)	Pore volume ($cc.g^{-1}$)
73S10C	275	Bimodal 4.5,7.5	0.326
63S20C	242	Bimodal 3.6,13.0	0.495
53S30C	275	Multimodal 3.7,5.5,15.6	0.762

Based on the obtained textural parameters (Table 7.1 and 7.4) on the pristine and SBF soaked samples, high silica and low CaO endures greater variations in surface area and this process favors the enhanced bioactivity of 73S10C mesoporous glass sample.

Based on the above analysis, we are now able to provide more qualitatively the possible origin of the formation of ACP followed by crystalline HCA layer in the studied MBG's and highlight the various factors influence on the apatite formation ability. The glass compositions chosen in the present work are close to the known bulk bioglass 45S5®, however, the local structural units present in the glass and glass-ceramic compositions are very much different as revealed by FTIR and NMR techniques. Therefore, we suggest that the formation of ACP has significant influence on the local structure of given glass and glass-ceramics in addition to their textural properties. The structure of bulk bioglass 45S5® has been characterized by the highly depolymerized fragment with various kinds of anionic species in which silicate species found to be Q^3, Q^2 and Q^0 and phosphate species are found to be in orthophosphate form [64]. The present structural investigations reveal that the silicate structure is less depolymerized (large Q^4 units) with minor amount of orthophosphate species due to the two reasons: (i) the modifier content is slightly less than 45S5 and (ii) intrinsically the sol-gel prepared samples have relatively less depolymerized nature than the corresponding bulk counterpart. Thus, the bioactivity of melt derived glasses is mainly determined by their chemical composition, whereas the apatite

formation in the MBG's is mainly controlled by their textural properties. Secondly, the MBG's contains high amount of silanol density which could play a crucial role on ACP formation than the composition of the glass. There are few reports to understand the effect of textural properties on the bioactivity in different type of glasses and in particularly, much work has been carried out in SiO_2-CaO-P_2O_5 glass system. Thus, we suggest that the obtained high Ca/P ratio in the present work stems from the superior textural property as well as the presence of different anionic species in the glass network structure.

In bulk glass samples, changing the chemical composition brings out the change in local atomic structure of the glass alone without any modification in the textural properties. The bioglass 45S5 comprises significantly larger amount of network modifier than present in MBGs thereby possessing depolymerized network built up of primarily by Q^2 silicate units (and to lesser extent Q^3 units). As proposed by Hill [65] that the optimal network connectivity (N_c) for MDBGs with $N_c \leq 2$ (bioglass 45S5 has an N_c of 1.9) but the same condition is not hold good for the sol-gel glasses, which are bioactive even with Nc around 3.7. In the present work, we find that the 73S10C glass is bioactive and show the high Ca/P ratio close to the 45S5 glass composition. Since, the MBG's are characterized by the high surface area and mesoporosity which leads to the complex nature of local atomic structure with wide range of Q species. Although the NMR studies on these glasses show the different type of Q^n species with high N_c (around 3.7), still it exhibits enhanced bioactivity due to the presence of large amount of hydroxyl groups [66].

Therefore, it is observed from the present investigation that, there exists a large variation in the local atomic structure of MBG and MDBG. The ^{29}Si NMR evidenced the presence of Q^4 and Q^3(OH) species after immersion in SBF although these species were not present in the as prepared bulk glass samples [67]. The emergence of Q^3(OH) and Q^4 species shows the reploymerization of silanols to form silica-rich layer and evidences the dissolution of glassy network. On the other hand, in the case of MBGs the surface is enriched with silanols and physiosorbed water molecules. Therefore, it has been proposed that the mechanism involved in HCA formation in MBG will be similar to Hench mechanism but with some important

differences [68]. Hence, the porosity and silanol density not only accelerates the first three stages of surface reaction but it may also even circumvent them. In addition to these crucial factors controlling the mechanism of bioactivity in MBG, presence of CaP cluster is also considerable.

Remarkably, we find that the substitution of CaO for SiO_2 inhibits the apatite formation on the surface of mesoporous glass [41]. Clearly, it is distinguishable that the bioactivities of glass samples are higher than the glass-ceramics, which consists of two phases apatite-like and wollastonite. This type of apatite/wollastonite (A/W) has been widely studied in several aspects and are said to be bioactive [69]. However, an earlier study indicated that the apatite growth ability of glasses are higher than A/W glass-ceramics [70] due to the structure of wollastonite, in which Ca^{2+} is readily linked to silicate network with less solubility [71]. Therefore, the presence of these two phases decreases the ion-dissolution process and hence leads to slow rate of apatite formation. Secondly, the textural property of glass ceramic is less superior to glasses under study which implies less amount of silanols formation in the glass-ceramic, which are nucleating sights for apatite and further slowing down of ion leaching process [72]. Ultimately, all these factors cause for the poor degree of apatite crystallization in glass-ceramic.

7.4 CONCLUSIONS

In this Chapter, we have investigated the relationship among the structure, texture and bioactivity of quaternary glass and glass-ceramic mesoporous system. The results obtained by various techniques before and after soaking in SBF corroborated the correlation among structural, textural and bioactivity. The silicate network got depolymerized to minor extent with increasing Ca^{2+} ions but not consumed by phosphate phase**.** However, the alkaline-earth richest composition displayed clear presence of Q^2_{Si}, Q^3_{Si}, and Q^4_{Si} species. The existence of calcium orthophosphate phase shows that this phase must be closely associated with the pore walls comprising nanometric-sized “inclusions” of similar phase. The high surface area in conjunction with the structural feature may be a possible explanation for experimentally observed enhanced bioactivity through the easy access of ions to the fluid. Owing to superior textural, structural and morphological characteristics, these glasses are promising materials for biomedical applications.

REFERENCES

[1] Hench, L.L. J. Am. Ceram. Soc. 74(1991)1487-1510.

[2] Vallet-Regi, M.; Ragel, C.V.; Salinas, A.J. Eur. J. Inorg. Chem. 6(2003)1029-1042.

[3] L.L. Hench, J. Am. Ceram. Soc. 81(1998)1705-28.

[4] L.L. Hench, R.J. Splinter, T.K. Greenlee, W.C. Allen, 2(1971)117-141.

[5] U. Gross, V.J. Strunz, Biomed. Mater. Res. 14(1980)607-618.

[6] T. Kokubo, S. Ito, M. Shingematsu, S. Sakka, T. Yamamuro, 20(1985)2001-2004.

[7] O.H. Andersson, L. Guizhi, K.H. Karlsson, L. Niemi, J. Miettinen, J. Juhanoja, J. Mater. Sci.: Mater. Med. 1(1990)219-227.

[8] S.A. Bagshaw, E. Prouzet, J.J. Pinnavaia, Science 269(1995**)**1242-1244.

[9] C. Yu, J. Fan, B. Tian, G.D. Stucky, D. Zhao, J. Phys. Chem. B, 107(2003)13368-13375.

[10] Q.Z. Chen, Y. Li, L.Y. Jin, J.M.W. Quinn, P.A. Komesaroff, Acta Biomater. 6(2010)4143-4153.

[11] C.T. Kresge, M.E. Leonowicz, W.J. Roth, J.C. Vartulli, J.S. Beck, Nature 359(1992) 710-712.

[12] M.E. Davis, Nature 417(2002)813-821.

[13] A. Stein, Adv.Mater. 15(2003)763-775.

[14] I. Izquierdo-Barba , L. Ruiz-Gonzalez, J.C. Doadrio, J.M. Gonzalez-Calbet, M. Vallet-Regi, Solid State Sci. 7(2005)983-989.

[15] X. Yan, X. Huang, C. Yu, H. Deng, Y. Wang, Z. Zhang, Biomaterial 27(2006)3396-3403.

[16] P. Horcajada, A. Ramila, K. Boulahya, J. Gonzalez-Calbet, M. Vallet-Regi, Solid State Sci. 6(2004)1295-1300.

[17] A. Lopez-Noriega, D. Acros, I. Izquierdo-Barba, Y. Sakamoto, O. Terasaki, M. Vallet-Regi, Chem. Mater. 18(2006)3137-3144.

[18] S.A. Bagshaw, E. Prouzet, J.J. Pinnavaia, Science 269(1995)1242-1244.

[19] J.C. Jansen, Z. Shan, L. Marehese, W. Zhou, N. vonder Puil, T. Maschmeyer, Chem. Commun. (2001)713-714.

[20] I. Lebecq, F. Desanglois, A. Leriche, C. Follet-Houttemane, J. Biomed. Mater. Res., Part A 83A (2007)156-168.

[21] P. Saravanapavan, J.R. Jones, R.S. Pyrce, L.L. Hench, J. Biomed. Mater. Res., PartA 66A(2003)110-119.

[22] K.S.K. Lin, Y.H. Tseng, Y. Mou, Y.C. Hsu, C.M. Yang, C.C. Chan, Chem. Mater. 17(2005)4493-4501.

[23] D. Acros, D.C. Greenspan, M. Vallet-Regi, J. Biomed. Mater. Res., PartA 65A(2003)344-351.

[24] C. Ohtsuki, T. Kokubo, T. Yamamuro, J. Non-Cryst. Solids 143(1992)84-92.

[25] H. Augiar, E.L. Solla, J. Serra, P. Gonzalez, B. leon, F. Malz, C. Jager, J. Non-Cryst. Solids 354(2008)5004-5008.

[26] V. Aina, F. Bonino, C. Morterra, M. Miola, C.L. Bianchi, G. Malavasi, M. Marchetti, V. Bolis, J. Phys. Chem. C 115(2011)2196-2210.

[27] I. Izquierdo-Barba, D. Acros, Y. Sakamoto, O. Terasaki, A. Lopez-Noriega, M. Vallet-Regi, Chem. Mater. 20(2008)3191-3198.

[28] A.J. Pedone, Phys. Chem. C 113(2009)20773-20784.

[29] A. Tilocca, A.N. Cormack, J. Phys. Chem. B 111 (2007)14256-14264.

[30] P.N. De Aza, A.H. De Aza, P. Pena, S. De Aza, Bol. Soc.Esp. Ceram. V. 46(2007)45-55.

[31] Y. Fan, Y. Piaaping , S.S. Huang , J.H. Jiang, H.Z. Lian, J.J. Lin Phys. Chem. C 113(2009)7826-7830.

[32] A. Martinez, I. Izquierdo-Barba, M. Vallet-Regi, Chem. Mater. 12(2000)3080-3088.

[33] A.Garcia, M. Cicuendez, I. Izquierdo-Barba, D. Acros, M. Vallet-Regi, Chem. Mater. 21(2009)5474-5484.

[34] M. Cerruti, D. Greenspan, K. Powers, Biomaterials 26(2005)1665-1674.

[35] P.Y.Shih, J.Y. Ding, S.Y. Lee, Mater. Chem. Phys. 80(2003)391-396.

[36] C. Dayanand, G. Bhikshamaiah, V.J. Tyagaraju, M. Slagram, A.S.R. Kirsihna Murthy ,J. Mater. Sci. 31(1996)1945-1967.

[37] M.R. Ahsan, M.G. Mortuza, J. Non-Cryst. Solids 351(2005)2333-2340.

[38] H. Aguiar, J. Serra, P. Gonzalez, B. Leon, J. Non-Cryst. Solids 355(2009)475-480.

[39] K.S.W.Sing, D.H. Everett, R.A.W.Haul, L. Moscou, R.A. Pierotti, J. Rouquerol, T. Siemieniewska, Pure & Appl. Chem. (1985) 57603-57619.

[40] A. Lucas-Girot, F.Z. Mezahi, M. Mami, H. Oudadesse, A. Harabi, M.L. Floch, J. Non-Cryst. Solids 357(2011)3322-3327.

[41] X. Li, X. Wang, D. He, J. Shi, J. Mater. Chem. 18(2008)4103-4109.

[42] X. Yan, X.Huang, C. Yu, H. Deng, Y. Wang, Z. Zhang, Biomaterials 27(2006)3396-3403.

[43] I. Elgayar, A.E. Aliev, A.R. Boccaccini, R.G. Hill, J. Non-Cryst. Solids 351(2005)173-183.

[44] S.C. Christiansen, D.Y. Zhao, M.T. Janicke, C.C. Landry, G.D. Stucky, B.F. Chmelka, J. Am. Chem. Soc. 123(2001)4519-4529.

[45] C.C. Liu, G.E. Maciel, J. Am. Chem. Soc. 118(1996)5103-5119.

[46] C. Mercier, C. Follet-Houttemane, A. Pardini, B. Revel, J. Non-Cryst. Solids 357(2011)3901-3909.

[47] H. Aguiar, J. Serra, P. Gonzalez, Int. J. Appl. Ceram. Technol. 8(2011)511-522.

[48] Y-H. Tseng, J. Zhan, K.S.K Lin, C-Y. Mou, J.C.C. Chan, Solid State Nucl. Magn. Reson. 26(2004),99-104.

[49] M. Circuendez, M.T. Portoles, I. Izquierdo-Barba, M. Vallet-Regi, Chem. Mater. 24(2012)1100-1106.

[50] M. O'Donnell, S.J. Watts, R.V. Law, R.G. Hill, J. Non-Cryst. Solids 354(2008)3554-3560.

[51] E. Leonova, I. Izquierdo-Barba, D. Acros, A. Lopez-Noriega, N. Hedin, M. Vallet-Regi, M. Eden, J. Phys. Chem. C 112(2008)5552-5562.

[52] S. Hayakawa, K. Tsuru, C. Ohtsuki, A. Osaka, J. Am. Ceram. Soc. 82(1999)2155-2160.

[53] P.N. Gunawidjaja, A.Y.H. Lo, I., Izquierdo-Barba, A. Garcia, D. Arcos, B. Stevensson, J. Grins, M. Vallet-Regi, M. Eden, J. Phys. Chem. C 114(2010)19345-19356.

[54] D. Acros, D.C.Greenspan, M. Vallet-Regi, J. Biomed. Mater. Res. 65A(2003)344-351.

[55] H.A. ElBatal, E.M.A. Khalil, Y.M. Hamdy, Ceram. Int. 35(2009)1195-1204.

[56] M. Braun, P. Hartmann, C. Jana, J. Mater. Sci. Mater. Med. 3(1995)150-154.

[57] H. Takadama, H-M. Kim, T. Kokubo, T, Nakamura, Chem. Mater. 13 (2001) 1108-1113.

[58] R. Ravarian, F. Moztarzadeh, M.S. Hashjin, S.M. Rabiee, P. Khoshhakhlagh, M. Tahriri, Ceram. Int. 36(2010)291-297.

[59] C. Vaid, S. Murugavel, R. Khashyap, R.P. Tandon, Micro. Meso. Mater. 159 (2012)17-23.

[60] I. Izquierdo-Barba, M. Colilla, M. Vallet-Regi, J. Nanomater. 3(2008)1-14.

[61] P. Horcajada, A. Ramila, K. Boulahya, J. Gonzalez-Calbet, M. Vallet-Regi, Solid State Sci. 6(2004)1295-1300.

[62] Y. Zhu, C. Wu, Y. Ramaswamy, E. Kockrick, S. Paul, S. Kaskel, H. Zreiqat, Micropor. Mesopor. Mater. 112(2008)494-503.

[63] H.M.M. Moawad, H. Jain, J. Am. Ceram. Soc. 90(2007)1934-1936.

[64] S. Murugavel, C. Vaid, V.S. Bhadram, C. Narayana, J. Phys. Chem. B. 114 (2010) 13381-13385.

[65] R.J. Hill, Mater. Sci. Lett. 15(1996)1122-1125.

[66] H.M. Kim, F. Miyaji, T. Kokubo, T. Nakamura, J. Biomed. Mater.Res.32(1996)409-417.

[67] E.Dietrich, H. Oudadesse, M.L. Floch, B. Bureau, T. Gloriant, Adv. Eng. Mater 11 (2009)B98-B105.

[68] I. Izquierdo-Barba, D. Acros, Y. Sakamoto, O. Terasaki, A. Lopez-Noriega, M. Vallet-Regi, Chem. Mater. 20(2008)3191-3198.

[69] K. Lin, M. Zhang, W. Zhai, H. Qu, J. Chang, J. Am. Ceram. Soc. 94(2011)99-105.

[70] C.V. Ragel, M. Vallet-Regi, L.M. Rodriguez-Lorenzo, Bioamterials, 23(2002)865-1872.

[71] N.J. Coleman, M. Bellantone, J.W. Nicholson, A.P. Mendham, Ceramics-Silikaty 51(2007)1-8.

[72] J. Wei, F. Chen, J. Shin, H. Hong, C. Dai, J. Su, C. Liu, Biomaterials 30 (2009) 1080-1088.